Available online at www.sciencedirect.com
SCIENCE DIRECT®
Journal of Solid State Chemistry 174 (2003) 132–140
JOURNAL OF SOLID STATE CHEMISTRY
http://elsevier.com/locate/jssc

# Formate incorporation in the structure of Ca-deficient apatite: Rietveld structure refinement

R.M. Wilson,* J.C. Elliott, and S.E.P. Dowker

*Dental Biophysics, Queen Mary, University of London, Medical Sciences Building, Mile End Road, London E1 4NS, UK*

Received 13 December 2002; received in revised form 19 March 2003; accepted 31 March 2003

**Abstract**

Two sets of non-stoichiometric apatites (Ca-deficient apatites) were prepared from calcium phosphate solutions by homogeneous precipitation through the hydrolysis of formamide at 95°C. One set of products contained monetite ($CaHPO_4$) and apatite, whilst the second, with more formamide, contained only apatite. Rietveld whole pattern fitting structure refinements were undertaken on all samples, and chemical analyses, IR and NMR spectroscopy, on the second set of samples. The Ca/P mol ratio was 1.596. Rietveld analysis gave lattice parameters $a = 9.4729(20)$ and $c = 6.8855(9)$ Å and showed that $Ca^{2+}$ ions were lost exclusively from Ca2 sites, and that the $PO_4$ tetrahedron volume and P–O bonds were 4.4% and 1.4% smaller, respectively, than in hydroxyapatite (OHAp). Formate, $HCO_2^-$, was clearly visible in the IR and NMR spectra, but the diffraction studies showed it was not present as a separate crystalline phase. Chemical analysis gave 5.8 wt % formate. We propose that the enlarged *a*-axis compared with OHAp ($a = 9.4243(55)$ Å) and reduced $PO_4$ dimensions and P occupancy are, respectively, caused by the partial replacement of $OH^-$ and $PO_4^{3-}$ ions in the structure by $HCO_2^-$ ions. These substitutions would parallel the similar known substitutions of $CO_3^{2-}$ ions in precipitated carbonate apatites.


*Keywords:* Apatite; Rietveld analysis; Formate; Hydroxyapatite; MAS NMR; FTIR; X-ray diffraction

## 1. Introduction

The mineral of bones and teeth is a poorly crystallized impure hydroxyapatite (OHAp), $Ca_{10}(PO_4)_6(OH)_2$. The mineral differs from OHAp as it contains a few percent carbonate, has a variable Ca/P mol ratio and contains variable amounts of acid phosphate. The Ca/P mol ratio of the mineral in dental enamel is generally less than 1.667, the value for stoichiometric OHAp, whilst for bone, it is usually greater than 1.667. Synthetic apatitic calcium phosphates can be precipitated with Ca/P mol ratios from below 1.5 to 1.667. These contain acid phosphate and are typically poorly crystallized with submicron sized crystals.

Although in the past, a Ca/P ratio lower than 1.667 has been attributed to the adsorption of $PO_4^{3-}$ ions on the surface of the apatite crystals, it is now generally believed that it originates from a loss of $Ca^{2+}$ ions from the unit cell, hence the name Ca-deficient apatites (Ca-def Aps) commonly given to these precipitates. Various general formulae have been proposed for the Ca-def Aps with Ca/P mol ratios from 8/6 to 10/6 (Table 3.2 in Ref. [1]). They all assume that the unit cell contains six phosphate ions and that charge balance is maintained by formation of $HPO_4^{2-}$ ions and in most cases also loss of $OH^-$ ions. In some formulae, $H_2O$ molecules occupy vacant $OH^-$ ion sites.

There is clear evidence for the presence of $HPO_4^{2-}$ ions in Ca-def Aps as the P–OH stretching mode at $\sim 870\,cm^{-1}$ in the infrared (IR) absorption spectrum increases as the Ca/P ratio falls [2,3]. Other evidence for $HPO_4^{2-}$ ions derives from the formation of pyrophosphate on heating at 400–600°C [4] by the reaction

$$2HPO_4^{2-} \rightarrow P_2O_7^{4-} + H_2O. \quad (1)$$

Ca-def Aps also weaker exhibit OH stretching and librational IR bands than OHAp (see Fig. 4 in Ref. [5]), which supports the loss of $OH^-$ ions from the unit cell.

The main quantitative support for the proposed unit cell formulae comes from estimating the $HPO_4^{2-}$ formed via measurement of the pyrophosphate formed in

*Corresponding author. Fax: +44-020-7377-7931.
*E-mail address:* r.m.wilson@qml.ac.uk (R.M. Wilson).

0022-4596/03/$ - see front matter © 2003 Elsevier Science (USA). All rights reserved.
doi:10.1016/S0022-4596(03)00188-9

Eq. (1) [4]. However, the pyrophosphate yield can be affected by secondary reactions. For example, formation of additional $HPO_4^{2-}$ through the reaction of $H_2O$ with $PO_4^{3-}$ [6] or loss of pyrophosphate through reaction with OHAp to form $\beta$-$Ca_3(PO_4)_2$ [4]. Difficulties in determining the unit cell contents means there can be no certainty about the structural formula for Ca-def Aps, nevertheless, the formula proposed by Winand [7]

$$Ca_{10-x}(HPO_4)_x(PO_4)_{6-x}(OH)_{2-x} \quad (2)$$

is commonly cited.

Precipitated Ca-def Aps usually have a similar $c$-axis parameter to OHAp made at high temperatures, but the $a$-axis parameter is typically increased by 0.01–0.02 Å [8], indicating that lattice substitutions do take place. Rietveld structure analysis by whole powder diffraction pattern methods [9] with X-ray diffraction (XRD) data has been used to study a series of variously precipitated Ca-def Aps [10]. Most samples had a greater total of X-ray scattering density in the $c$-axis channels than could be accounted for by $2OH^-$ ions per unit cell, but the authors were not able to attribute this unequivocally to the structural water thought to be present in these samples. The lattice parameters ranged from $a = 9.4157(2)$ and $c = 6.8777(2)$ for preparations with no $HPO_4^{2-}$ ions detectable by IR to $a = 9.4389(8)$ and $c = 6.8865(6)$ Å for preparations with easily detectable $HPO_4^{2-}$ [10].

Most studies of Ca-def Aps have been undertaken on submicron sized crystals. These had large surface areas that could adsorb substantial amounts of ions, so their composition probably did not accurately reflect the chemical composition of the unit cell. The small crystal size will also reduce the quality of diffraction patterns, and hence structure determinations based on them. Given these difficulties, coupled with the problems of determining the $HPO_4^{2-}$ ion content discussed earlier, it is not surprising that many structural formulae have been proposed for the Ca-def Aps. On the other hand, there are reports of the synthesis of Ca-def Aps with micron sized crystals. These methods use homogeneous precipitation through the slow release of $NH_3$ by hydrolysis of urea [11], formamide [12], or acetamide [12] at 80–95°C over a number of days. As these apatites are well-crystallized, the unit cell contents should be given by the chemical composition; they should also give good powder XRD patterns and hence good data for structure analysis by Rietveld refinement methods. Despite these potential advantages, there appears to have been little investigation of the structure of homogeneously precipitated Ca-def Aps. The aim of this study was to take advantage of the high crystallinity of Ca-def Aps precipitated homogeneously at 95°C, in this case using formamide, to attempt a detailed structure determination by Rietveld methods using powder XRD data.

## 2. Experimental

### 2.1. Sample preparation

The preparation followed that used by Yasukawa et al. [12]. Instead of the more common urea, these authors used formamide or acetamide which have the advantage that the absence of gaseous decomposition products, particularly $CO_2$, allows the preparation to take place in a closed system. Both the absence of evolved $CO_2$ and the closed system greatly reduce the possibility of $CO_3^{2-}$ ion inclusion in the structure, which is a common complicating contaminant. Formamide was used in the present preparations. Two batches under different precipitation conditions were made, selecting the formamide concentrations and hydrolysis times using Fig. 4A in Ref. [12]. Both conditions were selected to give OHAp alone, rather than a mixture of OHAp and monetite, the first being close to the condition for a mixture of OHAp and monetite (low formamide concentration, LF samples), and the second well away from it (high formamide concentration, HF samples).

Seven LF samples were prepared, D10–D16. For each sample, 4.002 g $NH_4NO_3$ and 5.904 g $Ca(NO_3)_2 \cdot 4H_2O$ were dissolved in 100 mL of $CO_2$-free deionized water. 1.981 g of $(NH_4)_2HPO_4$ were then added to give an overall Ca/P mol ratio of 1.667. The resulting precipitate of $CaHPO_4 \cdot 2H_2O$ was dissolved by adjusting the pH to 3.0 with 1 mol $dm^{-3}$ $HNO_3$ solution. The solution was put in a 250 mL polycarbonate conical flask with a Teflon magnetic stirrer in a water bath at 95°C (D10 was put in a polypropylene bottle without stirring), then 80 mL formamide were added. $N_2$ was bubbled through for a few seconds, the flask tightly stoppered and left for 4 days. The solution was filtered using filter paper in a conical funnel and the precipitates briefly washed. The samples were dried at 80°C for 4 h. D13 was lost, so only six samples were available for study.

For the HF samples, a single batch of solution was made using six times the above quantities in order to reduce the inter-sample variability. After adjusting to pH 3, the solution was divided into six equal volumes and the above procedure followed except that the formamide volume was increased to 112 mL and the hydrolysis time to 6 days. A polycarbonate flask was used for the first sample, but this was attacked by the increased concentration of formamide and lost. The remaining five samples (D18–D22 inclusive) used polypropylene flasks following Yasukawa et al. [12]. D18 was filtered with filter paper using a conical funnel. As this was very slow, the precipitate was not thoroughly washed. D19–D22 inclusive were filtered on a Buchner funnel under vacuum and thoroughly washed with deionized water. All samples were dried at 80°C for 4 h. Samples D20–D22 inclusive, but not D18 and D19,

were ground up before drying. The yields for both LF and HF syntheses were about 2 g.

Calcium formate (Merck Rectapur, min. 99%), monetite (Lumifax Ltd), hydroxyapatite SRM 2910 (Standard Reference Material 2910, National Institute of Standards and Technology (NIST), Gaithersburg, MD) and sodium formate (Aldrich Chemical Co., 99.998 wt%) were used as standards.

### 2.2. Methods for characterization

*Weight loss and chemical analyses.* The loss in weight of 40–80 mg duplicate samples of D18–D22 on heating at 900°C for 4 h was determined. Weight losses for D18 and D19 were about twice that of the other samples. As D18 and D19 had not been ground before drying at 80°C, they were redried at 80°C for 24 h after which losses at 900°C were in line with those of the other samples. These latter results are reported here. D20 and D21 were analyzed for formate by ion exclusion chromatography and samples heated at 900°C for 4 h were analyzed in duplicate by ICP-AES. SRM 2910 was analyzed at the same time, so that the results could be normalized to the values published by NIST for this standard. The chemical analyses were undertaken at the Natural History Museum, South Kensington.

*Infrared spectroscopy*. Fourier transform IR spectroscopy (FTIR) of the HF samples and standards (2 mg), dispersed in a KBr matrix (300 mg), were recorded using a PerkinElmer Spectrum GX FTIR spectrometer.

*Solid-state NMR*. The HF samples and standards were sent to the University of London NMR service at University College, London where $^{1}$H NMR spectra were run on a Brucker MSL-300 spectrometer. The $^{1}$H observational frequency was 300 MHz; there were 257 scans with a delay of 5 s and a magic angle spin speed of 6112 Hz for SRM 2910 and 12,000 Hz for all other samples. Shifts are given in parts per million (ppm) referenced to tetra methyl silane.

*X-ray diffraction.* Powder XRD patterns were collected from all samples, including the HF samples after heating to 900°C, following the procedure used earlier [13,14]. A 1500 W sealed tube with a Cu target (25 mA and 40 kV) was used with a Ge 111 monochromator to give Cu$K\alpha_1$ radiation ($\lambda = 1.5406$ Å). Diffraction patterns were collected with an INEL CPS-120 [15,16] curved position sensitive detector that allows simultaneous data collection in 4096 bins over 1–121° in $2\theta$. The sample holder was a (711) cut Si single crystal with the incoming monochromatic beam striking its surface at an angle of ~3.5° so as to minimize the background. Generally 5 mg samples were used. The sample holder was rotated about a fixed axis normal to its surface to increase the number of crystallites in differing orientations contributing to the powder pattern, thus obtaining a better powder average. Each data set was collected for at least 1000 min. The statistically poorest data set had around 30,000 counts per bin in the most intense region and a median (background) of over 2000 counts per bin. Patterns were calibrated using curves produced from lead nitrate run before and after each sample and of similar quality to the sample data set. The calibration curves were a least-squares spline fitted to the differences between the measured and calculated (using $a = 7.8586$ Å at ~20°C [17]) positions of the 29 most intense lead nitrate peaks between 19° and 117° in $2\theta$.

### 2.3. Rietveld analysis

The program GSAS [18] was used to refine the structures with form factors for neutral atoms. The background was modelled using Chebyschev polynomials of the first kind. The March–Dollase model for preferred orientation was used in all the refinements, but differed little from unity. The peakshape used was type 3 varying GU, GW, LX and trns. Starting atomic parameters for all apatite structures came from the refinement in $P6_3/m$ of Holly Springs OHAp using neutron data [19]. Occupancies and atom positions, and unit cell, peak profile, sample displacement and background parameters were allowed to vary. Following the previously used procedure for apatite Rietveld refinements, the Ca1 occupancy was fixed at the stoichiometric value [13,14]. The H occupancy was allowed to vary, but not its positional or displacement parameters. For D10 to D16, the relative phase fraction of monetite ($CaHPO_4$) was also refined using the structure from Catti et al. [20] with $P\bar{1}$ symmetry. It was found possible to vary the anisotropic displacement parameters in the final stage of the refinements (except for D14), but the matrix for O1 was always non-positive definite. However, the occupancies and positional parameters did not change very much. The results reported here are all from refinements in which the anisotropic displacement parameters were fixed to those reported for Holly Springs OHAp [19].

Because unit cell occupancies of stoichiometric OHAp determined from Rietveld analyses differ reproducibly from theoretical values by up to 5% [13,14], it is likely that measured occupancies of other apatites are similarly changed. Thus, correction factors from results for stoichiometric OHAp have been used to correct unit cell occupancies of other apatites under study [13,14]. The same procedure was applied here to the mean unit cell contents for the LF and HF samples. The correction factors were calculated from the mean of six OHAp results (penultimate entry in Table 3 of Ref. [14]).

The Ca/P ratio was determined from the well-known method of measuring the ratio of $Ca_3(PO_4)_2$ to OHAp formed on heating to 900°C [1]. Ca-def Aps decompose primarily to $\beta$-$Ca_3(PO_4)_2$ and OHAp, though $\alpha$-$Ca_3(PO_4)_2$ is sometimes formed [14], even though it is

not the stable polymorph below 1125°C [1]. The OHAp might also decompose partially to oxy-hydroxyapatite, particularly in a dry atmosphere [1]. The Ca/P mol ratios were calculated from the relative amounts of α-, β-$Ca_3(PO_4)_2$ and OHAp determined by Rietveld analyses. It was assumed the phases were stoichiometric; any small decomposition to oxy-hydroxyapatite was neglected as it would have had a negligible effect on the calculated contribution from apatite. In these refinements, the relative quantities of the three phases, lattice parameters, peak parameters and instrument zero were allowed to vary, but none of the structural parameters. The α-$Ca_3(PO_4)_2$ was modelled using its published structure [21]. Problems were found using the single-crystal X-ray structure for β-$Ca_3(PO_4)_2$ [22]. The powder pattern which best modelled the β-$Ca_3(PO_4)_2$ was obtained using the Rietveld determined structure of β-$(Ca,Mg)_3(PO_4)_2$ [23] with the Mg atoms replaced by Ca and with isotropic displacement parameters derived from the anisotropic displacement parameters for the single-crystal structure determination [22].

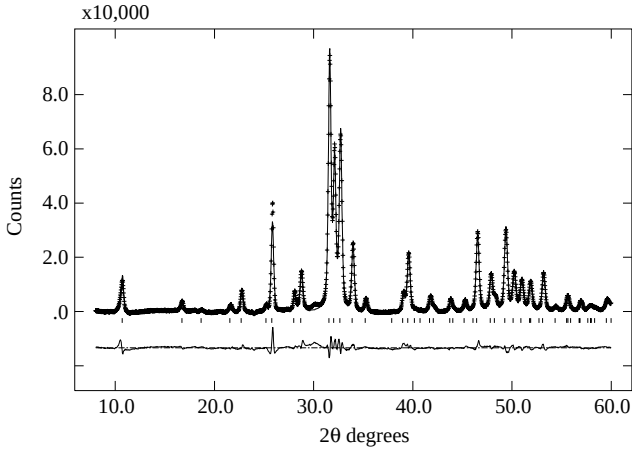


Fig. 1. X-ray powder diffraction pattern of HF sample D20 from 10–60° (2θ) (Cu$K\alpha_1$ radiation, 1240 min data collection time). + + + + + + experimental; — calculated for hexagonal OHAp. The tick marks are the expected peak positions for hexagonal OHAp. Occasional glitches on the trace originate from contamination on the detector anode, not the specimen.

## 3. Results and discussion

### 3.1. Crystalline phases present

Powder XRD showed that monetite, in addition to apatite, was present in all LF samples, but monetite could not be detected in the HF samples. Two non-apatitic weak lines (18° and a broad line at 30° in 2θ, Fig. 1) could be seen in all the HF samples. These are assigned to $Ca(OH)_2$ and poorly crystallized $CaCO_3$ (probably calcite) respectively. Presumably, the $Ca(OH)_2$ derived from the alkaline conditions used and some then reacted with atmospheric $CO_2$ to form $CaCO_3$. The monetite contents of the LF samples (D10–D12 and D14–D16) derived from Rietveld refinements were 7.40, 6.13, 5.33, 45.65, 26.89, and 18.20 wt% respectively, with apatite making up the 100 wt% total. XRD confirmed that HF samples after heating to 900°C contained only OHAp, α- and β-$Ca_3(PO_4)_2$. The α- and β-$Ca_3(PO_4)_2$ contents from Rietveld refinements for heated HF samples are given in Table 1 (columns 5 and 6). XRD confirmed that the calcium formate used as a reference example of a formate salt for IR and $^1$H NMR was α-$Ca(HCO_2)_2$.

### 3.2. Chemical analyses and weight loss data

No LF samples were analyzed chemically because of their substantial monetite contents (see above). Analyses and weight loss data for the HF samples are given in Table 1. The Ca/P ratios determined from Rietveld analysis (column 7) are very consistent with the Ca/P

Table 1
Chemical composition (ICP-AES) of HF samples heated 4 h at 900°C (columns 2, 3), wt% loss on heating from 4 h at 80°C to 4 h at 900°C (column 4), and α- and β-$Ca_3(PO_4)_2$ wt% (balance is OHAp) (columns 5, 6) after heating to 900°C. Ca/P mol ratio from α- and β-$Ca_3(PO_4)_2$ wt% (column 7) and from chemical analysis (column 8)

| 1 | 2 | 3 | 4 | 5 | 6 | 7 | 8 |
|---|---|---|---|---|---|---|---|
| No. | Ca wt% chem. | $PO_4$ wt% chem. | %wt loss | α-$Ca_3(PO_4)_2$ wt% | β-$Ca_3(PO_4)_2$ wt% | Ca/P mol. Riet. | Ca/P mol. Chem. |
| D18 | 39.86 | 58.96 | 8.80 | 14.62 | 25.59 | 1.597 | 1.602 |
| D19 | 39.45 | 58.51 | 8.65 | 19.35 | 23.34 | 1.592 | 1.598 |
| D20 | 39.20 | 58.24 | 8.05 | 22.19 | 21.02 | 1.591 | 1.595 |
| D21 | 39.35 | 58.45 | 7.77 | 19.04 | 23.68 | 1.592 | 1.595 |
| D22 | 39.30 | 58.16 | 7.33 | 13.80 | 26.90 | 1.596 | 1.601 |
| mean | 39.43 | 58.46 | 8.12 | 17.80 | 24.11 | 1.594 | 1.598 |
| σ | 0.23 | 0.28 | 0.55 | 3.14[a] | 2.01[a] | 0.002 | 0.003 |

[a] These standard deviations include variability due to changes in the balance between α- and β-$Ca_3(PO_4)_2$ formed. The mean (standard deviation) for the total α- plus β-$Ca_3(PO_4)_2$ is 41.91(1.35). The latter standard deviation excludes this variability and is much smaller, as expected.

ratios determined from the chemical composition (column 8) indicating that all the preparations are very similar and have a Ca/P mol ratio of 1.596, substantially less than stoichiometric OHAp (1.667). D20 and D21 contained 5.78 and 5.75 wt% $HCO_2^-$, respectively.

The mean weight loss on heating at 900°C can be used to calculate the composition of the samples dried at 80°C (Ca 36.23, $PO_4$ 53.71 wt%). The mean $HCO_2^-$ content was taken as the mean of the two determinations (5.76 wt%). These figures give a notional unit cell of

$$Ca_{9.59}(PO_4)_6(OH)_x + 1.36\,HCO_2^-, \quad (3)$$

where the number of $PO_4^{3-}$ ions is put equal to six to maintain structural integrity, following usual practice. The requirement for charge balance gives a value of $x$ of −0.18, but IR spectroscopy clearly shows the presence of acid phosphate that is not accounted for in Formula (3). The amount of acid phosphate is unknown, but little would be needed to require a significant number of $OH^-$ ions to be present.

As discussed later, there is evidence that the $HCO_2^-$ ions are located in both $PO_4^{3-}$ and $OH^-$ ion sites. There are clearly vacancies available in $OH^-$ sites, but Formula (3) has been scaled so that all $PO_4$ sites are occupied. However, if it is scaled so that the number of Ca(1) atoms equals the stoichiometric value (4), as done in the Rietveld analysis, then Formula (3) becomes

$$Ca(1)_4Ca(2)_{5.50}(PO_4)_{5.94}(HCO_2)_{0.06}(OH)_x(HCO_2)_{1.30}. \quad (4)$$

Clearly, the number of $HCO_2^-$ ions that can be accommodated in $PO_4$ sites depends critically on the scaling used.

### 3.3. Infrared spectroscopy

The IR spectra of HF samples D19–D22 inclusive were very similar. D20 is shown in Fig. 2 with assignments in Table 2. Additional bands were seen in D18 (strongest at 1694 and 1630 $cm^{-1}$) which are attributed to formamide contamination (amide I and II, respectively) due to insufficient washing. A significant feature of the spectra of the HF samples is the presence of additional bands, which are assigned to the formate ion, $HCO_2^-$, based on comparison with the published IR spectra of α- and β-$Ca(HCO_2)_2$ [24] (frequencies given in Table 2). The strongest band attributed to formate (1599 $cm^{-1}$) in Fig. 2 can also be seen rather indistinctly in a previously published spectrum of a similar preparation (Fig. 3, spectrum (a) in Ref. [12]), but the bands were not commented on.

The undistorted $HCO_2^-$ ion is planar, with $C_{2v}$ symmetry and six non-degenerate normal modes. The

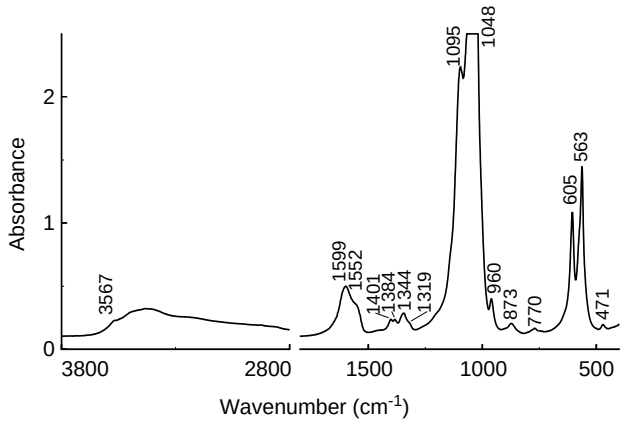


Fig. 2. FTIR spectrum of HF sample D20 with assignments in Table 2.

Table 2
Infrared frequencies ($cm^{-1}$) and assignments[a] for HF Ca-def Ap (Fig. 2, sample D20), and frequencies ($cm^{-1}$), assignments and intensities for α- and β-$Ca(HCO_2)_2$[b] (weak overtones and combination bands in the calcium formate spectra have been omitted)

| Frequency ($cm^{-1}$) | Assignment[c] | α-$Ca(HCO_2)_2$ | β-$Ca(HCO_2)_2$ |
|---|---|---|---|
| 471 | $\nu_2$ $PO_4^{3-}$ | | |
| 563 | $\nu_4$ $PO_4^{3-}$ | | |
| 605 | | | |
| 770 | $\nu_3$ O–C–O sym bend | 783 m<br>789 m<br>801 m<br>804 m | 790 s |
| 873 | P–(OH) stretch $HPO_4^{2-}$ | | |
| 960 | $\nu_1$ $PO_4^{3-}$ | | |
| Obscured | $\nu_6$ out–of–plane C–H bend | 1068 vw<br>1080 vw | Not seen |
| 1048[d] and 1095 | $\nu_3$ $PO_4^{3-}$ | | |
| 1319 sh | $\nu_2$ C–O sym stretch | 1353 s<br>1362 s | 1359 s |
| 1344 | | | |
| 1384 | $\nu_5$ in-plane C–H bend | 1389 s | 1383 s |
| 1401 | | 1401 s | |
| 1450 | $\nu_3$ $CO_3^{2-}$ | | |
| Trace? | | | |
| 1552 sh | $\nu_4$ C–O asym stretch | 1587 s<br>1629 sh ? | 1600 |
| 1599 | | 1658 sh ? | |
| 2000 | $2\nu_3$ $PO_4^{3-}$ | | |
| Trace | $\nu_1$ C–H sym stretch | 2869 w<br>2890 w | 2857 vw<br>2907 vw |
| 3000–3500 | O–H stretch $H_2O$ | | |
| 3567 sh | O–H stretch $OH^-$ | | |

[a] See Ref. [1] for references to assignments of apatite bands.
[b] Data for calcium formates from Ref. [24]; sh = shoulder, s = strong, m = medium, w = weak, vw = very weak and ? = uncertain assignment.
[c] When no ion is given, assignment is to formate, $HCO_2^-$; sym = symmetric, asym = asymmetric.
[d] Off-scale in Fig. 2.

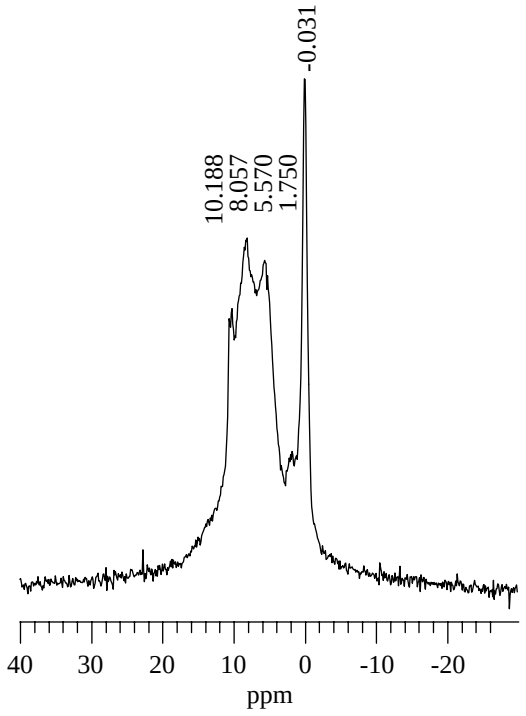


Fig. 3. $^1$H NMR spectrum of HF sample D21, see text for assignments.

common polymorph of calcium formate, $\alpha$-$Ca(HCO_2)_2$, has $HCO_2^-$ ions in two crystallographically different environments [25]. The $HCO_2^-$ fundamental bands in $\alpha$-$Ca(HCO_2)_2$ (Table 2) are doubled which was attributed [24] to the two environments with further splitting from correlation field effects. The IR spectrum of $\beta$-$Ca(HCO_2)_2$ is much simpler (Table 2) because the $HCO_2^-$ ions occupy only one site [24]. Table 2 shows that the formate bands in the HF samples are sufficiently different from those in $\alpha$- and $\beta$-$Ca(HCO_2)_2$ to establish that the formate is not present either as $\alpha$- or $\beta$-$Ca(HCO_2)_2$. This is supported by the observation noted earlier that apatite (apart from possible small amounts of $Ca(OH)_2$ and calcite) is the only crystalline phase seen in the XRD patterns of the HF samples. The $HCO_2^-$ spectrum in the HF samples possibly has doubled bands. This can be seen particularly for $\nu_5$, but may also occur for $\nu_4$ and $\nu_2$.

The most intense $CO_3$ band in precipitated carbonate-containing apatites is a broad doublet (1412 and 1465 $cm^{-1}$) due to $\nu_3$ [1]. There may be a very weak $\nu_3$ $CO_3$ band in the HF samples (Fig. 2), but there clearly can be little carbonate present, as expected from the mode of preparation. Thus the band at 873 $cm^{-1}$ (Table 2) can be assigned to the P–(OH) stretch of $HPO_4$ with negligible contribution from $\nu_2$ $CO_3$, the second most intense $CO_3$ band [1] which also absorbs near this frequency.

### 3.4. NMR spectroscopy

The $^1$H NMR spectra of D19–D22 inclusive were very similar. As with the IR spectrum, D18 had additional bands that are attributed to formamide impurities. The strongest additional peak was at 8.434 ppm and is assigned to amide protons. The spectrum of D21 is given in Fig. 3. Following Arends et al. [26] (their values in brackets), the sharp peak at −0.031 (−0.18) ppm is assigned to structural $OH^-$ ions and the peak at 5.570 (5.6) ppm to water molecules associated with the apatite. Arends et al. [26] reported a weak resonance at 1.5 ppm that they were unable to assign. A similar unassigned resonance is seen at 1.750 ppm in Fig. 3. The resonance at 8.057 ppm is assigned to the formate proton as we observed the strongest resonance in the $^1$H NMR spectrum of $\alpha$-$Ca(HCO_2)_2$ (not shown) to be at 8.315 ppm. The peak at 10.188 ppm (Fig. 3) might be due to $HPO_4^{2-}$ ions as a sample of brushite run under the same conditions had a strong peak at 10.435 ppm (not shown). However, Arends et al. [26] reported a weak resonance at 8.6 ppm that they thought was consistent with an assignment to an acidic phosphate proton. If this were present in Fig. 3, it would be masked by other peaks. Thus there is no confirmation for the presence of $HPO_4^{2-}$ ions from $^1$H NMR spectroscopy.

### 3.5. Rietveld refinement of Ca-def Ap structure

The standard deviations of the parameter means of the LF samples are much higher than for the HF samples (Tables 3 and 4). This indicates the lower quality of the LF compared with the HF refinements, presumably because of the substantial monetite content of the LF samples (see Results and Discussion under *Crystalline phases present*). Thus, individual results are reported only for the HF samples. However, the reported means for the LF samples are in good agreement with the HF samples.

The mean $a$-axis parameters for the HF and LF samples (9.4729(20) and 9.467(10) Å, respectively) are larger than for OHAp (9.4243(55) Å) and Ca-def Aps [1,8], whilst the $c$-axis parameters are essentially unchanged (Table 3, columns 3 and 4). Although an increase in the $a$-axis parameter is commonly seen in precipitated apatites, the increase found here is about 0.02 Å more than reported previously for the usual Ca-def Aps (see Introduction). However, an expansion of the $a$-axis parameter has been reported in apatites precipitated in the presence of $H_2O_2$ ($a = 9.500 \pm 0.002$ and $c = 6.875 \pm 0.002$ Å [27]). This expansion has been attributed to $O_2^-$ and other oxygen ions in the $c$-axis channels [28]. In the present case, IR and NMR spectroscopy clearly show the presence of $HCO_2^-$ ions, though there is no evidence for a separate crystalline phase. We therefore propose that at least part of the

Table 3
$R_{wp}$, lattice parameters and unit cell contents (scaled so that Ca1 is 4, the stoichiometric value) for HF samples and means for LF samples (standard deviations in brackets)

| 1 | 2 | 3 | 4 | 5 | 6 | 7 | 8 | 9 | 10 | 11 | 12 | 13 |
|---|---|---|---|---|---|---|---|---|---|---|---|---|
| No. | $R_{wp}$ | $a$ (Å) | $c$ (Å) | Ca2 | P | O1 | O2 | O3 | O(H) | H | $O_T$[a] | Ca/P[b] |
| D18 | 7.04 | 9.4752(7) | 6.8859(5) | 5.62(2) | 5.80(3) | 5.92(4) | 6.30(5) | 11.99(8) | 2.35(4) | 4.9(4) | 24.20 | 1.660 |
| D19 | 7.05 | 9.4716(8) | 6.8856(6) | 5.59(2) | 5.75(3) | 5.82(4) | 6.33(5) | 11.77(8) | 2.29(4) | 5.1(4) | 23.92 | 1.667 |
| D20 | 6.61 | 9.4740(8) | 6.8857(6) | 5.56(2) | 5.65(4) | 5.93(4) | 6.30(5) | 11.70(8) | 2.32(5) | 4.5(4) | 23.93 | 1.694 |
| D21 | 6.65 | 9.4737(7) | 6.8863(5) | 5.61(2) | 5.77(3) | 5.90(4) | 6.33(5) | 11.86(8) | 2.29(4) | 4.9(4) | 24.09 | 1.665 |
| D22 | 7.08 | 9.4702(7) | 6.8840(5) | 5.63(2) | 5.78(3) | 5.95(4) | 6.38(5) | 11.86(8) | 2.36(4) | 4.6(4) | 24.18 | 1.666 |
| Mean | — | 9.4729(20) | 6.8855(9) | 5.60(3) | 5.75(6) | 5.90(5) | 6.33(3) | 11.83(11) | 2.32(5) | 4.8(3) | 24.06(13) | 1.67(1) |
| HF corr mean[c] | — | — | — | 5.50(3) | 5.78(6) | 5.75(6) | 6.16(3) | 11.28(10) | 1.98(4) | 4.0(3) | 23.17(13) | 1.64(1) |
| LF corr mean[d] | — | 9.467(10) | 6.880(8) | 5.50(4) | 5.75(10) | 5.69(20) | 6.19(18) | 11.26(39) | 1.98(12) | 4.3(13) | 23.14(51) | 1.65(3) |
| OHAp[e] | — | 9.4243(55) | 6.8856(35) | 6.11(2) | 5.97(3) | 6.16(3) | 6.17(7) | 12.59(4) | 2.34(6) | 2.4(6) | 24.92 | 1.693 |

[a] $O_T = O1 + O2 + O3$.
[b] Mol ratio from occupancies in Rietveld structure refinements.
[c] Mean and standard deviation of occupancies for D18–D22 corrected with experimental occupancies for OHAp, see text.
[d] Mean and standard deviation for LF samples. Occupancies corrected with parameters for OHAp, see text.
[e] From mean and standard deviation (six samples) of OHAp parameters as given in penultimate row of Table 3 in Ref. [14].

Table 4
Positional parameters, mean (standard deviation) $\times 10^4$ for HF samples and means for LF samples and OHAp

| No. | Ca1$z$ | Ca2$x$ | Ca2$y$ | P$x$ | P$y$ | O1$x$ | O1$y$ | O2$x$ | O2$y$ | O3$x$ | O3$y$ | O3$z$ | O(H)$z$ |
|---|---|---|---|---|---|---|---|---|---|---|---|---|---|
| D18 | 0020(4) | 2481(2) | 9922(3) | 3987(3) | 3696(3) | 3332(6) | 4885(6) | 5807(6) | 4610(6) | 3423(5) | 2602(5) | 696(5) | 1816(18) |
| D19 | 0019(4) | 2472(2) | 9917(3) | 3983(3) | 3697(3) | 3333(6) | 4881(6) | 5807(6) | 4613(6) | 3416(5) | 2599(5) | 706(5) | 1827(18) |
| D20 | 0011(5) | 2475(3) | 9919(3) | 3985(3) | 3699(3) | 3309(6) | 4873(7) | 5795(7) | 4594(7) | 3425(5) | 2601(5) | 724(5) | 1847(20) |
| D21 | 0022(4) | 2475(2) | 9918(3) | 3984(3) | 3697(3) | 3322(5) | 4885(6) | 5798(6) | 4599(6) | 3426(5) | 2603(4) | 705(5) | 1845(18) |
| D22 | 0020(4) | 2474(2) | 9918(3) | 3986(3) | 3696(3) | 3326(6) | 4878(6) | 5805(6) | 4612(6) | 3423(5) | 2601(5) | 708(5) | 1808(17) |
| HF mean | 0018(4) | 2475(3) | 9919(2) | 3985(2) | 3697(1) | 3324(9) | 4880(5) | 5802(6) | 4606(9) | 3423(4) | 2601(2) | 708(9) | 1829(17) |
| LF mean | 0024(24) | 2467(14) | 9918(10) | 3983(14) | 3697(6) | 3339(24) | 4895(21) | 5808(16) | 4622(25) | 3427(19) | 2600(11) | 724(18) | 1833(24) |
| OHAp[a] | 11(4) | 2465(1) | 9926(2) | 3980(2) | 3676(2) | 3276(5) | 4850(5) | 5846(4) | 4629(8) | 3414(4) | 2559(6) | 683(5) | 1935(13) |
| HF mean-OHAp | 7 | 10 | −7 | 5 | 21 | 52 | 30 | −44 | −23 | 9 | 42 | 25 | −106 |
| LF mean-OHAp | 13 | 2 | −8 | 3 | 21 | 37 | 45 | −38 | −7 | 13 | 41 | 41 | −102 |

[a] Mean for six OHAp samples, last row of Table 1 [14].

increase in the $a$-axis parameter is caused by a partial replacement of $OH^-$ ions by $HCO_2^-$ ions in the $c$-axis channels, analogous to the well-known [1] partial replacement of $OH^-$ by $CO_3^{2-}$ ions in precipitated $CO_3$Aps. That $HCO_2^-$ ions can be located in the $c$-axis channels is not surprising as the $HCO_2^-$ ion has a similar size and shape as the $CO_3^{2-}$ ion (see later).

Unit cell contents from Rietveld structure refinements scaled to have four Ca1 atoms per unit cell are given in Table 3. Individual results and uncorrected means for the HF samples show an excess of O2 (column 8) and marked deficiency of P (column 6), which is inconsistent with the $PO_4$ tetrahedron. Application of the OHAp correction factors reduces the O2 excess slightly, but the P occupancy is still 3.7% too low. This is also reflected in the fact that the corrected occupancies for HF give a mean Ca/P ratio of 1.64(1) (Table 3, column 13) which is 2.7% larger than the ratio from Rietveld phase analysis of samples heated to 900°C and chemical analyses (1.594(2) and 1.598(3), Table 1, columns 7 and 8, respectively). The apparently low P occupancy might, in part, be associated with imperfect modelling of static disorder as a result of vacancies and substitutions in the structure. This possibility could be investigated by comparison of neutron diffraction studies at room and liquid helium temperatures. However, the low P occupancy could also be consistent with partial replacement of $PO_4^{3-}$ by $HCO_2^-$ ions (see later).

Turning to the other sites, there is a preferential loss (8.0%) of $Ca^{2+}$ ions from Ca2 sites over Ca1 sites. A preferential loss of Ca2 has also be found in Ca-def Aps precipitated at 80–95°C via the hydrolysis of urea (Wilson, Elliott, Dowker and Rodriguez unpublished results). Both the O(H) and H occupancies (Table 3, columns 10 and 11) are substantially higher than the stoichiometric values (2 and 2), indicating additional scattering in the hexad axis channel. Similar additional hexad axis scattering has been seen in dental enamel [13], precipitated carbonate [14] and carbonate-free [10] apatites where it has been attributed to $H_2O$ molecules.

It is also possible that some of this additional scattering arises from $HCO_2^-$ ions located on the hexad axis as discussed earlier.

Positional parameters for the HF and LF Ca-def Aps, together with OHAp for comparison, are given in Table 4. The largest shift is in $z$ for O(H) (−0.0106 for mean HF), which shows that the OH ion is 0.073 Å further away from the mirror plane at $z = \frac{1}{4}$ than in OHAp. Such shifts away from the mirror plane of 0.079 and 0.048 Å are also seen in dental enamel [13] and in a $CO_3$Ap formed in an aqueous slurry of calcite and monetite [14], respectively. Almost all the $x$ and $y$ shifts are positive (Table 4), which means that the atoms near the hexad axis are further away from the axis in Ca-def Ap compared with OHAp. This is consistent with the earlier deduction from the occupancies that the main differences in the Ca-def Ap structure from OHAp are the loss of Ca2 and the likely presence of water and/or formate in the hexad axis.

Details of the geometry of the $PO_4$ tetrahedron in the HF and LF samples with OHAp for comparison are given in Table 5. The principal changes from OHAp are a slight increase in distortion indices and slight reduction in size. The angle index changes most, followed by the edge index as would be expected if the P atom was shifted off the centroid whilst keeping the bond lengths more or less constant. As regards the contraction of the $PO_4$ tetrahedron, the decrease from OHAp in P–O1, P–O2, P–O3 and volume for the HF means are (from Table 5) 1.03%, 2.08%, 1.37% and 4.36% respectively. For comparison, P–O bond lengths and $PO_4$ volumes are listed in Table 6 for a variety of apatites that differ only with respect to the anion in the $c$-axis channels except dental enamel which also has a partial replacement of $PO_4^{3-}$ by $CO_3^{2-}$ ions. Dental enamel ($CO_3$ content about 3 wt%) has the smallest sum of P–O bond lengths and $PO_4$ volume, and clearly lies outside the normal range. This reduced size has been attributed to the partial replacement of $PO_4^{3-}$ by the smaller $CO_3^{2-}$ ion [13]. Such a contraction has also been observed in other apatites where this replacement is thought to takes place [14,30]. Table 6 shows that the P–O bond lengths and $PO_4$ volumes for HF and LF Ca-def Aps also lie well outside the normal range, suggesting there must again be some specific cause of the observed contraction in the $PO_4$ tetrahedron. This cannot be $CO_3^{2-}$ ions as these are not observed in the IR spectrum. It is therefore proposed that this contraction is caused by $HCO_2^-$ ions replacing $PO_4^{3-}$ ions in the lattice.

It is not surprising that $HCO_2^-$ ions, like $CO_3^{2-}$ ions, appear to be able to replace both $OH^-$ and $PO_4^{3-}$ ions in the apatite structure because the shape and dimensions of the $HCO_2^-$ and $CO_3^{2-}$ ions are very similar. Both ions are planar or nearly so. The $HCO_2^-$ ion has idealized bond angles O1–C–O2, O1–C–H and O2–C–H of 130.6°, 114.7° and 114.7° and bond lengths C–O1, C–O2 and C–H of 1.273, 1.273 and 1.153 Å, respectively [31]. The undistorted $CO_3^{2-}$ ion has $D_{3h}$ symmetry with a C–O bond length of 1.282 Å in calcite [32]. The O–O

Table 6
Calculated sums of P–O bond lengths and $PO_4$ volumes for various apatites

| Apatite | Sum of four P–O bond lengths (Å) | Vol. (Å$^3$) |
|---|---|---|
| Dental enamel [13] | 6.067 | 1.787 |
| LF Ca-def Ap[a] | 6.065 | 1.784 |
| HF Ca-def Ap[a] | 6.078 | 1.797 |
| FAp[b] [33] | 6.145 | 1.858 |
| Holly Springs OHAp[c] [19] | 6.140 | 1.853 |
| Synthetic OHAp[a] | 6.169 | 1.879 |
| ClAp[d] (*a*) [34] | 6.135 | 1.847 |
| ClAp[d] (*b*) [34] | 6.135 | 1.847 |
| ClAp[d] (*c*) [34] | 6.137 | 1.849 |
| BrAp[e] [35] | 6.152 | 1.859 |

[a] Table 5, this work.
[b] Synthetic fluorapatite.
[c] Neutron diffraction.
[d] The three non-equivalent ions (*a*, *b* and *c*) in synthetic monoclinic chlorapatite.
[e] Synthetic bromapatite.

Table 5
$PO_4$ bond lengths (Å), volume (Å$^3$) and distortion indices for the HF samples and means for HF, LF and OHAp

| No. | P–O1 | P–O2 | P–O3 | $PO_4$ vol. | Bond[a] × $10^2$ | Angle[a] × $10^2$ | Edge[a] × $10^2$ |
|---|---|---|---|---|---|---|---|
| D18 | 1.534(6) | 1.493(5) | 1.533(4) | 1.811(8) | 0.99 | 1.45 | 1.23 |
| D19 | 1.525(6) | 1.496(5) | 1.529(4) | 1.799(8) | 0.79 | 1.51 | 1.17 |
| D20 | 1.536(7) | 1.485(5) | 1.520(4) | 1.780(9) | 0.99 | 1.91 | 1.75 |
| D21 | 1.538(6) | 1.489(5) | 1.527(4) | 1.800(8) | 1.04 | 1.71 | 1.54 |
| D22 | 1.531(6) | 1.492(5) | 1.526(4) | 1.795(8) | 0.88 | 1.51 | 1.28 |
| HF mean | 1.533(5) | 1.491(4) | 1.527(5) | 1.797(11) | 0.94 | 1.62 | 1.39 |
| LF mean | 1.534(22) | 1.497(25) | 1.517(11) | 1.784(16) | 0.98 | 1.84 | 1.57 |
| OHAp[b] | 1.5490 | 1.5227 | 1.5482 | 1.8791 | 0.63 | 1.5 | 1.2 |
| $\sigma$[b] | 0.0026 | 0.0034 | 0.0041 | 0.0075 | 0.15 | 0.08 | 0.04 |

Standard deviations are given in parentheses.
[a] P–O tetrahedral bond, angle and edge distortion indices as defined by Baur [29].
[b] Mean and standard deviation for six OHAp samples, last entry of Table 2, Ref. [14].

distances in $HCO_2^-$ and $CO_3^{2-}$ are therefore 2.313 and 2.220 Å, respectively, whilst the O–O distance in the apatite $PO_4^{3-}$ ion is 2.506 Å (mean of four independent distances from neutron diffraction study of Holly Springs HAp [19]). Presumably the oxygen atoms of the $HCO_2^-$ ion occupy positions near the vacated oxygen sites of the $PO_4^{3-}$ ion.

## 4. Conclusion

A set of Ca-def Aps essentially free of $CO_3$ have been prepared via the hydrolysis of formamide. NMR and IR spectroscopy and chemical analysis showed that formate ions were present, although no crystalline formate phase could be seen by XRD. Rietveld whole X-ray pattern fitting unexpectedly showed an enlarged *a*-axis and a $PO_4$ tetrahedron that was apparently smaller than in pure OHAp and a reduced P occupancy. It is proposed that these dimensional changes result, respectively, from partial replacement of $OH^-$ and $PO_4^{3-}$ ions by $HCO_2^-$ in the apatite structure, analogous to the similar known substitutions of $CO_3^{2-}$ ions in $CO_3$Aps. Chemical analysis confirmed the deficiency of $Ca^{2+}$ ions and IR the presence of $HPO_4^{2-}$ ions. Rietveld analysis showed that the $Ca^{2+}$ ions were lost from Ca2, rather than Ca1 sites in the lattice.

## Acknowledgments

This work was supported by the UK Medical Research Council Grant No G9824467.

## References

[1] J.C. Elliott, Structure and Chemistry of the Apatites and Other Calcium Orthophosphates, Elsevier, Amsterdam, 1994.
[2] J.A.S. Bett, L.G. Christner, W.K. Hall, J. Am. Chem. Soc. 89 (1967) 5535–5541.
[3] S.J. Joris, C.H. Amberg, J. Phys. Chem. 75 (1971) 3172–3178.
[4] A. Gee, V.R. Deitz, J. Am. Chem. Soc. 77 (1955) 2961–2965.
[5] E.E. Berry, J. Inorg. Nucl. Chem. 29 (1967) 317–327.
[6] B.O. Fowler, E.C. Moreno, W.E. Brown, Arch. Oral Biol. 11 (1966) 477–492.
[7] L. Winand, Ann. Chim. Ser. 13 6 (1961) 941–967.
[8] O.R. Trautz, Ann. New York Acad. Sci. 60 (1955) 696–712.
[9] R.A. Young (Ed.), The Rietveld Method, Oxford University Press, Oxford, 1993.
[10] R.A. Young, D.W. Holcomb, Calcif. Tissue Int. 34 (Suppl. 2) (1982) S17–S32.
[11] A. Mortier, J. Lemaitre, L. Rodrique, P.G. Rouxhet, J. Solid State Chem. 78 (1989) 215–219.
[12] A. Yasukawa, H. Takase, K. Kandori, T. Ishikawa, Polyhedron 13 (1994) 3071–3078.
[13] R.M. Wilson, J.C. Elliott, S.E.P. Dowker, Am. Mineral. 84 (1999) 1406–1414.
[14] H. Morgan, R.M. Wilson, J.C. Elliott, S.E.P. Dowker, P. Anderson, Biomaterials 21 (2000) 617–627.
[15] J. Ballon, V. Comparat, J. Pouxe, Nucl. Instr. Meth. Phys. Res. 217 (1983) 213–216.
[16] M. Evain, P. Deniard, A. Jouanneaux, R. Brec, J. Appl. Cryst. 26 (1993) 563–569.
[17] H. Nowotny, G. Heger, Acta Crystallogr. C 42 (1986) 133–135.
[18] A.C. Larson, R.B. Von Dreele, GSAS, General Structure Analysis System, Los Alamos National Laboratory Report LAUR 86-748, Los Alamos, 1986.
[19] K. Sudarsanan, R.A. Young, Acta Crystallogr. B 25 (1969) 1534–1543.
[20] M. Catti, G. Ferraris, A. Filhol, Acta Crystallogr. B 33 (1977) 1223–1229.
[21] M. Mathew, L.W. Schroeder, B. Dickens, W.E. Brown, Acta Crystallogr. B 33 (1977) 1325–1333.
[22] B. Dickens, L.W. Schroeder, W.E. Brown, J. Solid State Chem. 10 (1974) 232–248.
[23] A. Bigi, G. Falini, E. Foresti, A. Ripamonti, M. Gazzamo, N. Roveri, Z. Kristallogr. 211 (1996) 13–16.
[24] C.J.H. Schutte, K. Buijs, Spectrochim. Acta 20 (1964) 187–195.
[25] N. Burger, H. Fuess, Acta Crystallogr. B 33 (1977) 1968–1970.
[26] J. Arends, J. Christoffersen, M.R. Christoffersen, H. Eckert, B.O. Fowler, J.C. Heughebaert, G.H. Nancollas, J.P. Yesinowski, S.J. Zawacki, J. Cryst. Growth 84 (1987) 515–532.
[27] D.R. Simpson, Am. Mineral. 54 (1969) 560–562.
[28] J. Dugas, C. Rey, J. Phys. Chem. 81 (1977) 1417–1419.
[29] W.H. Baur, Acta Crystallogr. B 30 (1974) 1195–1215.
[30] J.C. Elliott, R.M. Wilson, S.E.P. Dowker, in: T.C. Huang (Ed.), Advances in X-ray Analysis, Vol. 45, International Centre for Diffraction Data, Newtown Square, PA, 2002, pp. 172–181.
[31] P.C.H. Mitchell, R.P. Holroyd, S. Poulston, M. Bowker, S.F. Parker, J. Chem. Soc. Faraday Trans. 93 (1997) 2569–2575.
[32] R. Wartchow, Z. Kristallogr. 186 (1989) 300–302.
[33] K. Sudarsanan, P.E. Mackie, R.A. Young, Mater. Res. Bull. 7 (1972) 1331–1337.
[34] P.E. Mackie, J.C. Elliott, R.A. Young, Acta Crystallogr. B 28 (1972) 1840–1848.
[35] J.C. Elliott, E. Dykes, P.E. Mackie, Acta Crystallogr. B 37 (1981) 435–438.